THE JOURNAL OF BIOLOGICAL CHEMISTRY VOL. 289, NO. 52, pp. 35757–35769, December 26, 2014

Asymmetrical Macromolecular Complex Formation of Lysophosphatidic Acid Receptor 2 (LPA_2) Mediates Gradient Sensing in Fibroblasts*[S]

Received for publication, July 15, 2014, and in revised form, November 4, 2014 Published, JBC Papers in Press, November 5, 2014, DOI 10.1074/jbc.M114.595512

Aixia Ren[‡1], Changsuk Moon[‡§1], Weiqiang Zhang[‡¶], Chandrima Sinha[‡], Sunitha Yarlagadda[‡§], Kavisha Arora[‡§], Xusheng Wang[‖], Junming Yue[‡], Kaushik Parthasarathi[‡], Rick Heil-Chapdelaine[**], Gabor Tigyi[‡], and Anjaparavanda P. Naren[‡§2]

From the [‡]Department of Physiology, University of Tennessee Health Science Center, Memphis, Tennessee 38163, the [§]Division of Pulmonary Medicine, Department of Pediatrics, Cincinnati Children's Hospital Medical Center, Cincinnati, Ohio 45229, the [¶]Department of Pediatrics, University of Tennessee Health Science Center, Memphis, Tennessee 38103, the [‖]Department of Structural Biology and Developmental Neurobiology, St. Jude Children's Research Hospital, Memphis, Tennessee 38105, and [**]Olympus America Inc., Center Valley, Pennsylvania 18034

Background: Chemotaxis is a fundamental process in many physiological and pathological events.
Results: An LPA gradient induces a spatiotemporally restricted decrease in the mobility of LPA_2 indicative of its cytoplasmic anchorage to NHERF2, the cytoskeleton and PLCβ, which causes a gradient of localized Ca^{2+} puffs.
Conclusion: Asymmetrical macromolecular complex formation by LPA_2 mediates gradient sensing.
Significance: Our finding provides a new mechanistic basis to help understand chemotactic gradient sensing.

Chemotactic migration of fibroblasts toward growth factors relies on their capacity to sense minute extracellular gradients and respond to spatially confined receptor-mediated signals. Currently, mechanisms underlying the gradient sensing of fibroblasts remain poorly understood. Using single-particle tracking methodology, we determined that a lysophosphatidic acid (LPA) gradient induces a spatiotemporally restricted decrease in the mobility of LPA receptor 2 (LPA_2) on chemotactic fibroblasts. The onset of decreased LPA_2 mobility correlates to the spatial recruitment and coupling to LPA_2-interacting proteins that anchor the complex to the cytoskeleton. These localized PDZ motif-mediated macromolecular complexes of LPA_2 trigger a Ca^{2+} puff gradient that governs gradient sensing and directional migration in response to LPA. Disruption of the PDZ motif-mediated assembly of the macromolecular complex of LPA_2 disorganizes the gradient of Ca^{2+} puffs, disrupts gradient sensing, and reduces the directional migration of fibroblasts toward LPA. Our findings illustrate that the asymmetric macromolecular complex formation of chemoattractant receptors mediates gradient sensing and provides a new mechanistic basis for models to describe gradient sensing of fibroblasts.

Chemotaxis is a fundamental process in many physiological and pathological events, including embryonic development, angiogenesis, wound healing, inflammation, and metastasis. The capacity of cells to sense and respond to a chemoattractant gradient is central to chemotaxis. This response is achieved by integrating chemoattractant signals originating from a family of G-protein-coupled receptors (GPCRs),[3] leading to dynamic organizational changes in signal transduction networks (1). In order to elucidate the mechanism of chemotaxis, two key questions must be answered. (i) What molecular events are initiated when a cell encounters a chemotactic gradient with as little as a 2% concentration difference across the cell perimeter? (ii) What is the dynamic process of signal amplification? The cells respond to external gradient signals by activation of chemoattractant receptors, which in turn initiates the intracellular signaling network, leading to directional motility (2–5). The crucial step in this response is how the low level and spatially distinct activation of GPCRs can provide the cell with an unambiguous cue for gradient sensing. Accumulating evidence suggests that the spatial organization of signaling molecules regulates chemotaxis (6–8). Previous studies of chemotaxis have shown that signaling events are restricted to the leading edge of the cell although chemoattractant receptors are uniformly distributed on the entire cell surface during migration (9). Recent studies utilizing fluorescence resonance energy transfer (FRET) methods have shown that the leading edge of *Dictyostelium discoideum* exhibits elevated cAMP receptor-mediated activation of the G proteins (10, 11). Single-particle tracking (SPT) imaging revealed that the dynamic properties of the cAMP GPCRs were involved in such gradient sensing (12, 13). These observations suggest that gradient sensing was initiated from a

* This work was supported, in whole or in part, by National Institutes of Health Grants DK080834 and DK093045 (to A. P. N.) and CA092160 (to G. T.).
[S] This article contains supplemental Videos 1–5.
[1] Both authors contributed equally to this work.
[2] To whom correspondence should be addressed: Division of Pulmonary Medicine, Dept. of Pediatrics, MLC2120 3333 Burnet Ave., Cincinnati Children's Hospital Medical Center, Cincinnati, OH 45229. Tel.: 513-803-4731; Fax: 513-803-4783; E-mail: anaren@cchmc.org.

[3] The abbreviations used are: GPCR, G-protein-coupled receptor; LPA, lysophosphatidic acid; PDZ, postsynaptic density-95/discs large/zona occludens-1; PLC-β3, phospholipase C-β3; QD, conjugated quantum dot; SPT, single-particle tracking; TIRF, total internal reflection fluorescence; DKO, double knock-out; MEF, mouse embryo fibroblast; CI, chemotactic index; RWD, relative wound density; MSD, mean square displacement; KS-test, Kolmogorov-Smirnov test; ERM, ezrin-radixin-moesin; EGFP, enhanced green fluorescent protein.

polarization in receptor activation in this organism. Until now, due to unresolved technical difficulties, the chemical gradient-induced activation pattern of chemoattractant receptors in fibroblasts has not yet been directly reported.

The sensitivity of gradient sensing is governed by signal amplification and adaption mechanisms. *Dictyostelium* and neutrophils perform strong internal signal amplification by means of feedback loops composed of phosphoinositide 3-kinase (PI3K) and its catalytic product, phosphatidylinositol 3,4,5-trisphosphate. It has been established that an early indicator of gradient sensing is the localized accumulation of phosphatidylinositol 3,4,5-trisphosphate that is accomplished through the regulation of PI3K and the PTEN (phosphatase and tensin homolog) activity at the leading edge (14). However, defective phosphatidylinositol 3,4,5-trisphosphate signaling was found only to affect the motility and not the chemotaxis of neutrophils (15) and *Dictyostelium* (16). Several types of cancer cells retain a highly invasive capacity despite loss of PTEN function, implying that chemoattractant sensing can be achieved independently of phosphatidylinositol 3,4,5-trisphosphate levels (17). Recently, a newly discovered pathway involving phospholipase A2 has been shown to mediate chemotaxis in cells lacking PI3K (18). These findings support the possibility that either there are multiple, redundant gradient-sensing mechanisms, or there is a common upstream compass coupled to redundant pathways of translating output into directional cell migration.

Calcium is known to play important roles in regulating cell migration (19, 20). Wei *et al.* (21) provided evidence that transient Ca^{2+} microdomains, known as Ca^{2+} flickers, are enriched near the leading edge of a motile fibroblast and that the asymmetry of Ca^{2+} flickers steers cells to turn. Highly localized Ca^{2+} elevations have been observed to trigger both attractive and repulsive growth cone turning (22). A study in zebrafish primordial germ cells found that transient Ca^{2+} elevations can locally induce protrusion formation (23). These studies support a model in which Ca^{2+} is a critical component in steering cells along a chemical gradient. Recent studies showed that depletion of extracellular Ca^{2+} disrupts the positive feedback loop that can be measured by either PI3K activity, actin polymerization, or protein kinase C (PKC) localization at the leading edge of polarized cells (24). Taken together, these observations suggest that Ca^{2+} gradients are indispensable to the positive feedback for gradient sensing of chemotactic cells.

The chemotactic migration of fibroblasts can be triggered by chemoattractants, including platelet-derived growth factor (PDGF) and LPA. LPA is one of the major motility-stimulating factors present in blood and other biological fluids. Although there has been great progress in understanding PDGF-induced chemotaxis in fibroblasts, the mechanisms of LPA-induced chemotactic migration remain poorly understood. LPA-initiated cellular responses are mediated through at least six GPCRs: LPA_1/Edg2, LPA_2/Edg4, LPA_3/Edg7, LPA_4/GPR23, LPA_5/GPR92, and LPA_6/P2Y5 (25). Recent studies have established that LPA_2 mediates the migration of several types of cancer cells (26–28). In this paper, we report our findings that an asymmetric activation of LPA_2 on the plasma membrane of fibroblasts elicits an asymmetric formation of macromolecular complexes of LPA_2, NHERF2 (Na^+/H^+ exchange regulatory factor 2), and phospholipase C-β3 (PLC-β3) that, through an intracellular signal amplification mechanism, trigger the formation of spatially restricted, short lived, and high frequency Ca^{2+} microdomains (Ca^{2+} puffs), which govern the LPA gradient sensing and directional motility of fibroblasts.

EXPERIMENTAL PROCEDURES

Materials—Heat-inactivated fetal bovine serum (FBS) and CO_2-independent medium were purchased from Invitrogen. Dulbecco's modified Eagle's medium (DMEM), 1-oleoyl-*sn*-glycero-3-phosphate (LPA, 18:1), 1-oleoyl-*rac*-glycero (oleoyl glycerol), fibronectin, and puromycin were purchased from Sigma-Aldrich. PLC-β inhibitor U73122 and its inactive analog U73343 and Polybrene were purchased from Santa Cruz Biotechnology, Inc. Anti-LPA_2 antibody (rabbit 2143) and anti-NHERF2 antibody (rabbit 2346) were generated by Genemed Synthesis, Inc. (San Antonio, TX). Anti-PLC-β3 antibody was purchased from Abcam (Cambridge, MA).

Cell Culture, Transfection, and Lentivirus Infection—NIH 3T3 cells were purchased from ATCC (Manassas, VA). NIH 3T3 cells were transfected with an N-terminal FLAG-tagged WT-LPA_2 construct (3T3-LPA_2 cells) or the L351A PDZ motif mutant LPA_2 (3T3-L351A cells). Double knock-out (DKO) mouse embryonic fibroblasts (MEFs), derived from *Lpar1*$^{-/-}$ and *Lpar2*$^{-/-}$ DKO mice and therefore deficient in LPA_1 and LPA_2, were reconstituted with either WT-LPA_2 (DKO-LPA_2 MEFs) or L351A-LPA_2 (DKO-L351A MEFs) as described previously (29). Cells were cultured in DMEM supplemented with 100 units/ml penicillin, 100 μg/ml streptomycin, and 10% FBS. The transfection was conducted using Lipofectamine 2000 (Invitrogen) according to the manufacturer's instructions. The FLAG-WT-LPA_2 and FLAG-L351A-LPA_2 lentiviral vectors were generated by the Viral Vector Core (University of Tennessee Health Science Center). Half-confluent cells were cultured in medium with 5 μg/ml Polybrene to which lentiviral vector was added and incubated overnight. After infection, cells were selected using 2 μg/ml puromycin for 5 days and used for experiments.

siRNA targeting NHERF2 was purchased from Santa Cruz Biotechnology. NIH 3T3 cells or DKO-LPA_2 MEFs at 50% confluence were transfected with 200 pM NHERF2 siRNA using Lipofectamine 2000. As a control, a scrambled 21-nucleotide RNA duplex was used. Twenty-four hours after transfection, cells were used for experiments.

Chemotactic Stimulation of Cells Using an LPA Gradient Released from a Micropipette—Cells were seeded on fibronectin-coated glass-bottomed dishes, starved for 6 h, and then incubated in CO_2-independent medium. Cells were stimulated by an LPA gradient generated by a micropipette at 37 °C. Micropipettes were prepared by pulling borosilicate capillaries to 1.0-mm outer diameter and 0.58-mm inner diameter on a dual stage glass micropipette puller (Narishige Co. Ltd., London). The micropipettes were filled with 200 nM LPA solution. The movement of cells was recorded using a Hamamatsu EM-CCD camera (C9100; Hamamatsu, Bridgewater, NJ) equipped on a phase-contrast microscope. The trajectories were analyzed using Slidebook version 5.0 software. The chemotactic index

(CI) was calculated by taking the cosine of the angle between a line directly up the gradient and one that connects a cell's starting point to its end point. A value of 1 is directly up the gradient, whereas a CI of 0 indicates motion perpendicular to the direction of the gradient.

High Content Microscopy—Cells were grown for 24 h in fibronectin-coated 96-well Essen BioScience (Ann Arbor, MI) ImageLock microplates in a CO_2 incubator. Wounds were made precisely using the 96-pin Wound-Maker provided with the IncuCyte™ system (Essen Bioscience) (30). After washing thoroughly with PBS to remove detached cells, the remaining cells were placed in the instrument in serum-free medium with or without LPA (1 μM), PLCβ inhibitor U73122 (2 μM), or its inactive analog U73343 (2 μM). The wound images were automatically acquired at 30-min intervals. The kinetics of the relative wound density (RWD) was analyzed using IncuCyte™ software.

Wound Healing Assay—Cells were grown on fibronectin-coated 35-mm diameter dishes and starved for 6 h prior to wounding. The wounds were made by scraping with a microtip. After being washed three times, cells were incubated in normal medium with or without 1 μM LPA for 6 h. A total of three different DKO, DKO-LPA$_2$, and DKO-L351A MEF cultures were analyzed, and experiments were repeated four times. Cells were imaged using an Olympus (Center Valley, PA) IX51 inverted microscope.

Coimmunoprecipitation and Immunoblotting—For coimmunoprecipitation of LPA$_2$, NHERF2, and PLC-β3, 3T3-LPA$_2$ and DKO-LPA$_2$ cells were starved in serum-free DMEM for 6 h and then stimulated with different concentrations of LPA for 5 min. After treatment, cells were harvested and resuspended in lysis buffer. The lysate was spun at 12,000 rpm for 10 min at 4 °C. The clear supernatant was subjected to immunoprecipitation using α-FLAG beads (Sigma-Aldrich) overnight at 4 °C. The immunoprecipitated beads were washed three times with lysis buffer, and proteins were eluted from the beads using 5× Laemmli sample buffer. The proteins were separated on 4–15% SDS-polyacrylamide gradient gels and immunoblotted for LPA$_2$, NHERF2, and PLC-β3 using the respective antibodies.

SPT and Data Analysis—3T3-LPA$_2$ and 3T3-L351A cells were grown on 35-mm fibronectin-coated glass-bottomed dishes (MatTeK, Ashland, MA). Cells were washed twice with serum-free medium and then incubated with biotin α-FLAG antibody (1 μg/ml; Sigma-Aldrich) for 30 min after an initial block (DMEM containing 4% BSA, 10 min) and washed five times, followed by a second incubation with streptavidin-conjugated quantum dots (QDs; Qdot-655, 0.1 nM; Invitrogen) for 5 min. Cells were washed with DMEM without phenol red for 6–10 min and immediately mounted on an Olympus inverted microscope (IX51) equipped with a ×100 oil immersion objective (numerical aperture = 1.4) and xenon (300-watt lamp) light source. Images were captured with a Hamamatsu EM-CCD camera at 10 frames/s for ~2 min. QD excitation and emission was controlled by a Qdot 655-A BrightLine® high brightness and contrast single-band filter set (Semrock, Rochester, NY). Acquisition of images and trajectory analysis were performed using SlideBook version 5.0 software. Single QDs were identified by characteristic blinking, and periods where the fluorescence signal disappeared due to the blinking of single QDs were omitted from the analysis. The trajectory was reconstructed by joining trajectory fragments immediately before and after the dark period of the blink. Trajectories were considered for 10 or more consecutive frames. The mean square displacement (MSD) of a trajectory was calculated using SlideBook version 5.0 software. The diffusion coefficients (D) were calculated with the equation, MSD = $4Dt$ using an analysis software and fitting the first 4–50 time points of the MSD curves *versus* the lag time.

Quantitation of LPA$_2$ Internalization—Cells were plated on glass-bottomed dishes for internalization assays. The cells were serum-starved for 6 h and then incubated with biotin-α-FLAG primary antibody for 30 min after initial block with 4% BSA, followed by a second incubation with streptavidin-conjugated QDs for 5 min. Cells were then rinsed and processed for time lapse microscopy to measure LPA$_2$ internalization.

Ca^{2+} Imaging with Non-fluorescent Acetoxymethyl Ester (Fluo-4 AM)—Cultured DKO, DKO-LPA$_2$, or DKO-L351 MEFs were loaded with 5 μM Fluo-4 AM in the presence of 1.5 μM pluronic acid F-127 and incubated for 30–45 min at 37 °C in the dark in KREB buffer, washed, and equilibrated for de-esterification for 15 min. Fluorescence images of Fluo-4 were acquired with 1 frame/s using the ×10 objective at 37 °C. The fluorescence intensity of Fluo-4 for each region of interest was divided by the averaged resting fluorescence intensity of 10 frames before stimulation of the same region, after which the background fluorescence was subtracted. The resultant relative fluorescence intensity (F/F_0) was used as an indicator of intracellular Ca^{2+} levels ($[Ca^{2+}]_i$). Image processing and analysis were performed using NIH Image software.

Total internal reflection fluorescence (TIRF) microscopy imaging of changes in $[Ca^{2+}]_i$ was performed in an in-house built TIRF microscopy system based on an Olympus microscope with a ×100 oil objective. Fluo-4 AM was excited at 488 nm, and images of emitted fluorescence were captured at a resolution of 128 × 128 pixels (1 pixel = 0.33 μm) at 60 frames/s with an EM-CCD camera. After subtraction of background, fluorescence intensity within a defined circular region of interest was expressed as F/F_0, where F is the fluorescence intensity at time t, and F_0 is the average fluorescence intensity from the same region of interest collected from the first ~10 frames.

Statistical Analyses—The Kolmogorov-Smirnov test (KS-test) was used to evaluate the differences between the different populations of the determined D. Statistical analyses also were performed using a two-tailed, unpaired Student's t test. Results are presented as mean ± S.E., and differences were considered statistically significant at $p < 0.05$.

RESULTS

LPA Gradient Induces a Spatially Restricted Reduction in the Mobility of LPA$_2$ in the Plasma Membrane—The dynamics of GPCRs in the plasma membrane and its relationship with receptor function are important to the actively developing field of research. In order to analyze the mobility of receptors in detail, it is necessary to monitor an individual receptor. We engineered an LPA$_2$ construct containing a FLAG tag at the N

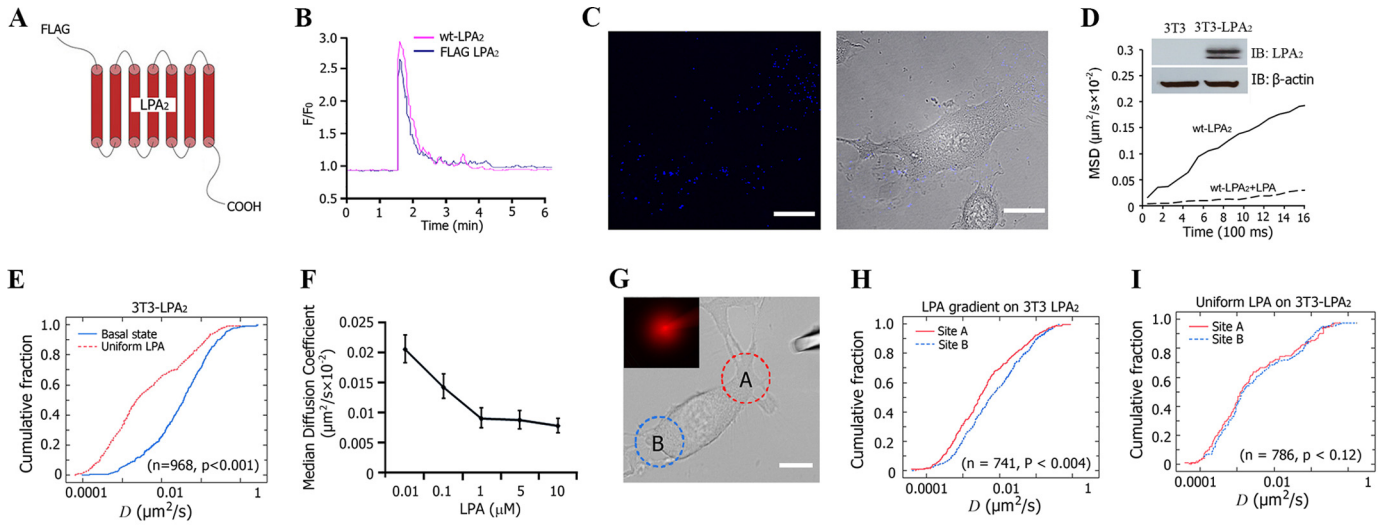

FIGURE 1. **Lateral mobility of LPA$_2$ on the plasma membrane of cells.** *A*, schematic representation of FLAG-tagged LPA$_2$. *B*, FLAG-LPA$_2$ functioned the same as WT-LPA$_2$ in LPA-induced intracellular Ca^{2+} mobilization. *C*, *left*, fluorescence image of 3T3-LPA$_2$-stable cells labeled with QDs. *Right*, phase-contrast image. *Scale bar*, 10 μm. *D*, MSD *versus* time plots for FLAG-LPA$_2$ in 3T3-LPA$_2$ cells at basal (without LPA) or LPA (1 μM)-activated state. Plots are averaged from 16–36 individual trajectories. The *inset blots* show the expression of LPA$_2$ in 3T3-LPA$_2$ cells. *E*, comparison of cumulative fraction plots from a KS-test of the difference in the diffusion coefficient (*D*) of LPA$_2$ at the basal state or after exposure to uniform LPA. The respective number of trajectories (*n*) and *p* value are listed. *F*, lateral mobility of LPA$_2$ in response to different concentration of LPA treatment. *G*, a representative image of a cell exposed to an LPA gradient generated by placing a micropipette releasing LPA (200 nM) in close proximity to a cell. Sites A and B (*A* and *B*) are designated relative to the site of micropipette. The *inset* shows the gradient generated by including fluorescent dextran in the pipette. *Scale bar*, 10 μm. *H*, comparison of the cumulative fraction plot from the KS-test of the difference in the diffusion coefficient of LPA$_2$ in site A and site B after exposure to an LPA gradient. The respective number of trajectories (*n*) and *p* value are listed. *I*, comparison of cumulative fraction plot from the KS-test of the difference in the diffusion coefficient of LPA$_2$ in site A and site B after exposure to uniformly distributed LPA. The respective number of trajectories (*n*) and *p* value are listed. *IB*, immunoblot; *Error bars*, S.E.

terminus (Fig. 1*A*) and tested its function using an intracellular calcium mobilization assay in rat hepatoma cells (RH777, an LPA-receptor null cell line). We found that cells transiently expressing FLAG-tagged LPA$_2$ exhibited the same function as non-tagged WT-LPA$_2$-expressing cells (Fig. 1*B*). We then used the SPT method to monitor the dynamic properties of LPA$_2$ in living fibroblasts. The membrane localization of LPA$_2$ labeled with streptavidin-conjugated QDs in 3T3-LPA$_2$ cells was observed (Fig. 1*C*). The expression of FLAG-tagged LPA$_2$ was confirmed by Western blotting (Fig. 1*D*, *inset*). Time lapse imaging showed the diffusion of LPA$_2$ confined at the plasma membrane during the 2-min observation period with a median diffusion coefficient (D_{med}) of ~0.0301 ± 0.0610 $\mu m^2/s$, which is typical for many membrane proteins, including GPCRs. Exposure to 1 μM LPA within seconds reduced the D_{med} of LPA$_2$ 13-fold to 0.0023 ± 0.0013 $\mu m^2/s$ (Fig. 1*D* and supplemental Video 1). The KS-test revealed a significant difference in the lateral mobility of LPA$_2$ between the basal and LPA-activated states (Fig. 1*E*). We next examined whether the LPA effect was dose-dependent and found that LPA decreased the lateral mobility of LPA$_2$ in a dose-dependent manner within the range of 10 nM to 1 μM (Fig. 1*F*). At ~100 nM of LPA, the D_{med} of LPA$_2$ reached half of that without LPA stimulation. At 1 μM LPA, the stimulation rose to a plateau; further increase in LPA concentration did not elicit a significant decrease in LPA$_2$ mobility.

We next examined the effect of an LPA gradient on the lateral mobility of LPA$_2$ by placing a micropipette releasing LPA in close proximity to a cell. To verify the establishment of an LPA gradient, we included fluorescent dextran in the micropipette with LPA and used the fluorescence intensity to calculate the gradient (Fig. 1*G*). Under our experimental conditions, we created >10% gradient steepness across the cell. After exposure to this LPA gradient, SPT data indicated that the lateral mobility of LPA$_2$ in the portion facing the LPA source (site "A") was more restricted, indicated by a significantly lower *D*, than that of LPA$_2$ in the portion farthest away from the LPA source (site "B") (Fig. 1*H*). In contrast, when the cells were exposed to LPA uniformly, the lateral mobility of LPA$_2$ in site A *versus* site B was indistinguishable (Fig. 1*I*). This suggests that the LPA gradient induced a spatially polarized reduction in the mobility of LPA$_2$, which reflects the spatial differences in ligand exposure of LPA$_2$ at different sites of the plasma membrane.

Chemoattractant receptors are uniformly distributed along the cell surface during cheomotaxis. However, some proteins can relocalize during cell migration, such as PTEN dissociating along the leading edge and accumulating at the cell rear during chemotaxis (14, 31). We studied the cellular distribution of LPA$_2$ during chemotaxis by transiently overexpressing an EGFP-tagged LPA$_2$ (Fig. 2*A*). A calcium mobilization assay in RH777 cells showed that EGFP-LPA$_2$ functioned similarly to WT-LPA$_2$ (Fig. 2*B*). TIRF microscopy imaging was used to examine the distribution of EGFP-LPA$_2$ with or without an LPA gradient stimulation. We found that EGFP-LPA$_2$ was distributed evenly throughout the plasma membrane regardless of whether an LPA gradient was present (5-min treatment) or not (Fig. 2*C*), suggesting that the LPA gradient-induced polarized decrease in LPA$_2$ mobility was not due to redistribution of LPA$_2$.

Internalization of several types of GPCRs occurs in response to agonist activation and can cause a redistribution of receptors away from the plasma membrane. LPA$_1$ has been reported to undergo ligand-induced internalization (32). In contrast, the ligand-induced internalization of LPA$_2$ has not been reported.

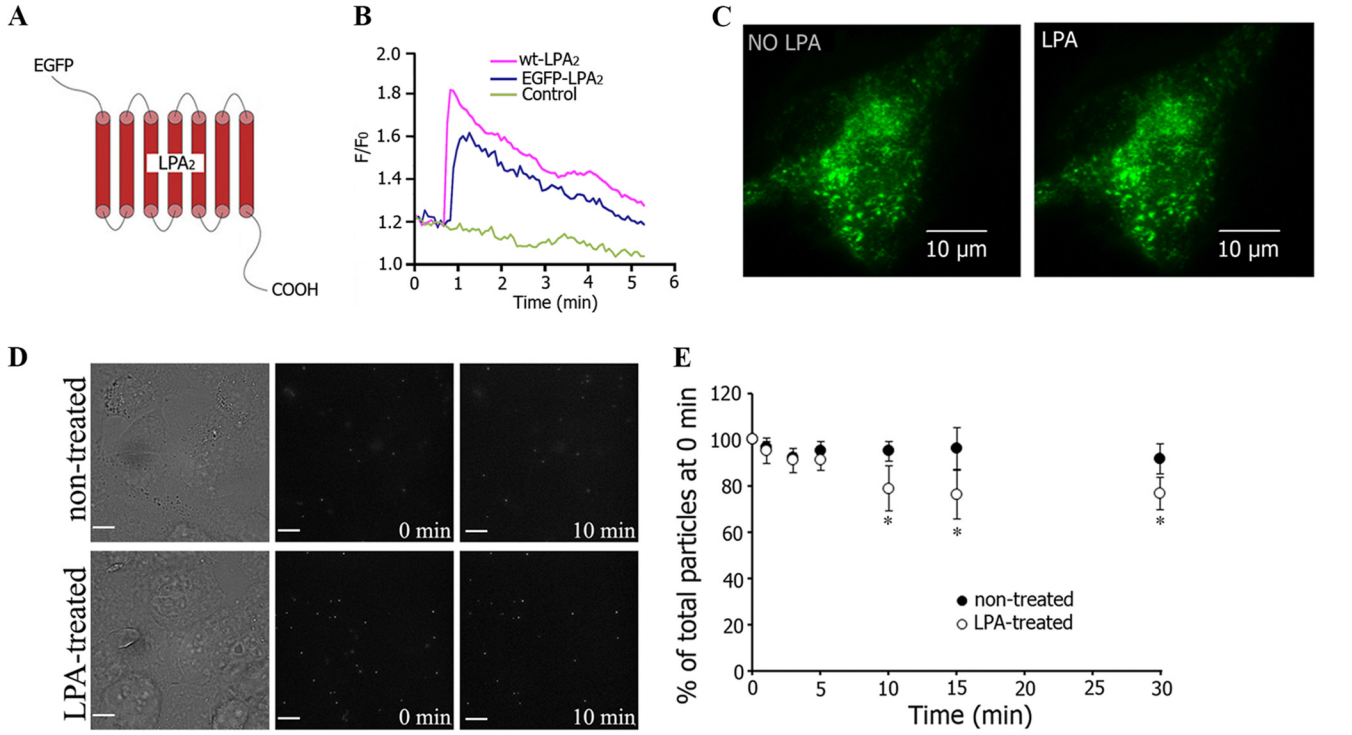

FIGURE 2. **LPA did not induce LPA$_2$ internalization within 5 min of exposure.** *A*, schematic representation of EGFP-tagged LPA$_2$. *B*, EGFP-LPA$_2$ functioned similar as WT-LPA$_2$ in LPA-induced intracellular Ca^{2+} mobilization. *C*, TIRF imaging showing the distribution of EGFP-LPA$_2$ in 3T3-LPA$_2$ cells before and after treatment with an LPA gradient for 5 min. *Scale bar*, 10 μm. *D*, SPT images of FLAG-LPA$_2$ expressed in HEK293 cells in the absence or presence of LPA. *Scale bar*, 10 μm. *E*, quantitative analysis of the percentage of LPA$_2$ internalization for 30 min with or without LPA treatment (mean ± S.E. (*error bars*), $n = 4$). *, significant differences compared with 0 min in each group ($p < 0.05$).

We investigated whether internalization of LPA$_2$ would occur upon exposure to LPA stimulus by using time lapse microscopy. HEK293 cells overexpressing FLAG-LPA$_2$ were labeled with biotin-α-FLAG primary antibody and then streptavidin-conjugated QDs. The cells were subjected to fluorescence time lapse microscopy with (5 μM LPA for maximal stimulation) or without LPA (Fig. 2*D*). The maximal stimulation of LPA$_2$ induced no detectable LPA$_2$ internalization within the first 5 min of exposure (Fig. 2*E*), although changes in receptor dynamics and receptor-activated Ca^{2+} responses were robustly triggered in the cells. Internalization of LPA$_2$ became detectable only after 10 min of stimulation and affecting only 25% of the receptors expressed uniformly on the cell surface (Fig. 2*E*). These observations emphasize the discordant time course of receptor dynamics that was apparent as early as 2 min of LPA application, and LPA$_2$ internalization was absent during the first 10 min of stimulant exposure. Taken together, our data suggest that the spatial regulation of the membrane dynamics of ligand-activated LPA$_2$ preceded the partial internalization of this receptor.

LPA Gradient Induces Congruent Spatiotemporal Patterns of Localized Ca^{2+} Microdomains in Fibroblasts—Our results thus far had indicated that an LPA gradient induced a mirroring decrease in the lateral mobility of LPA$_2$ along the length of the cells without a detectable change in the number of receptors present in the plasma membrane. We next examined how this spatiotemporal change of LPA$_2$ mobility is translated into localized intracellular signaling. LPA can activate changes in intracellular Ca^{2+} levels ($[Ca^{2+}]_i$) through receptor-mediated PLC activation (33). We used time lapse imaging to investigate the spatiotemporal patterns of $[Ca^{2+}]_i$ in Fluo-4 AM-labeled DKO MEFs that were reconstituted with WT-LPA$_2$ (DKO-LPA$_2$ MEFs) or L351A-LPA$_2$ (DKO-L351A MEFs). Note that DKO MEFs do not express LPA$_1$, LPA$_2$, or LPA$_3$ receptors and do not develop Ca^{2+} transients when exposed to LPA unless reconstituted with WT-LPA$_2$ or L351A-LPA$_2$ (29, 34). The expression of FLAG-tagged LPA$_2$ was confirmed by Western blot (Fig. 3*E*, *inset*). Exposure of Fluo-4 AM-labeled DKO-LPA$_2$ MEFs to an LPA gradient revealed that the transient fluorescence intensity of Fluo-4 increased in every cell (Fig. 3*A* and supplemental Video 2). In most cells, this $[Ca^{2+}]_i$ signaling initiated from the region nearest to the micropipette source of LPA. Using TIRF imaging, we observed that LPA elicited localized and short-lived high frequency Ca^{2+} microdomains analogous to Ca^{2+} puffs (35). These Ca^{2+} puffs rapidly triggered Ca^{2+} waves along the LPA gradient throughout the DKO-LPA$_2$ MEFs (Fig. 3*B* and supplemental video 3). Thus, DKO-LPA$_2$ MEFs can spatiotemporally sense and respond to an LPA gradient by directionally organized changes in $[Ca^{2+}]_i$ signals.

We further investigated the spatiotemporal properties of the LPA-elicited Ca^{2+} puffs by dividing the cell into two regions of equal area, proximal and distal in relation to the position of the micropipette (Fig. 3*C*). Analysis of the occurrence of Ca^{2+} puffs showed higher incidences in the proximal region (nearer to the micropipette, region labeled *a*) than that in the distal region (away from the micropipette, region labeled *b*) (Fig. 3*D*). This observation suggested that the LPA gradient induced asymmetric LPA$_2$ receptor activation and caused a Ca^{2+} puff gradient

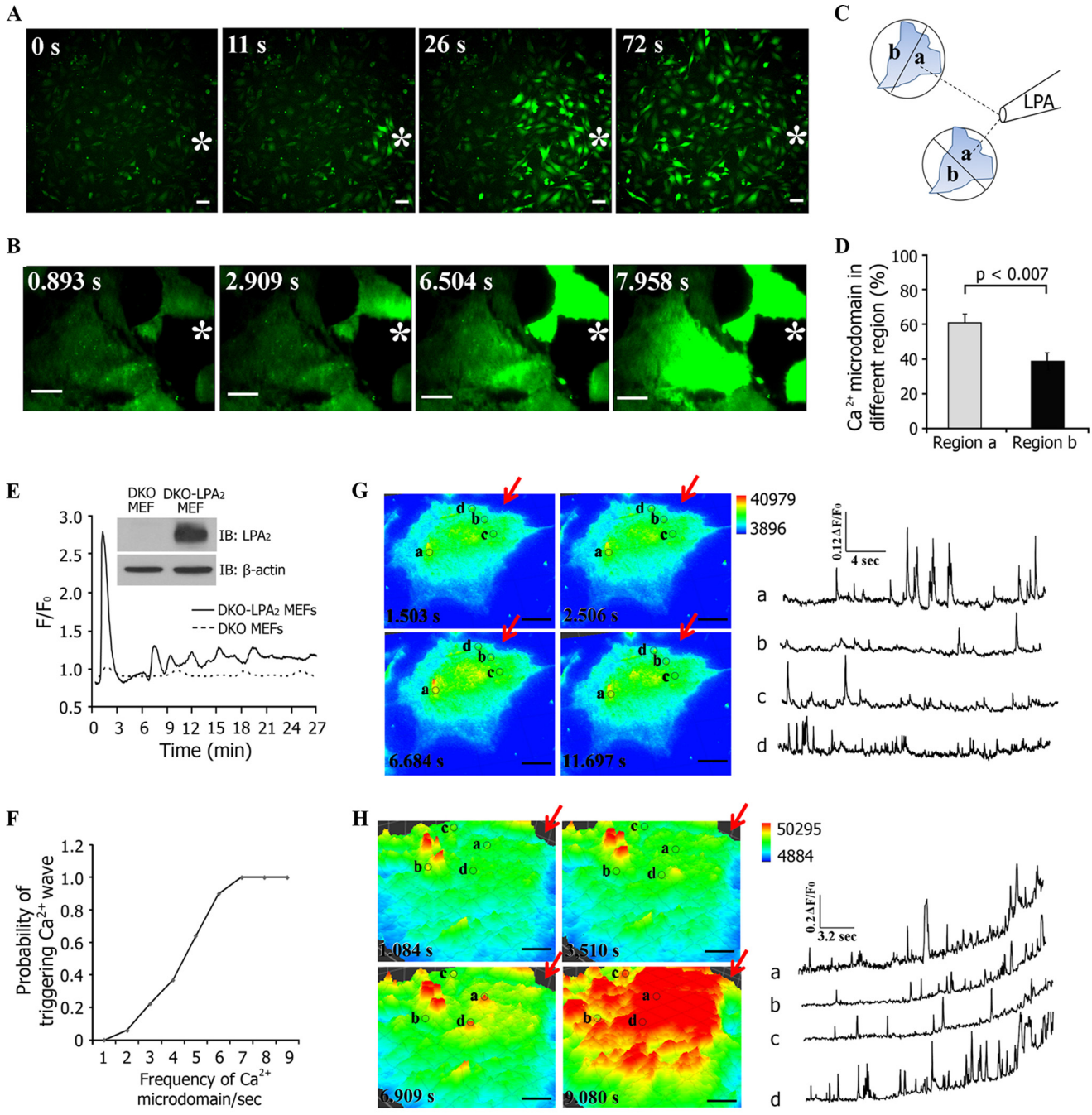

FIGURE 3. **Spatiotemporal patterns of intracellular Ca^{2+} puffs stimulated by an LPA gradient.** *A*, Fluo-4 AM fluorescence images of $[Ca^{2+}]_i$ responses in DKO-LPA$_2$ MEFs exposed to an LPA gradient emitted by a micropipette containing 200 nM LPA. *Scale bar*, 50 μm. *B*, TIRF imaging of Fluo-4 AM-stained DKO-LPA$_2$ MEFs exposed to an LPA gradient produced by a micropipette containing 200 nM LPA. *Scale bar*, 10 μm. *White stars*, sites of the micropipette. *C*, *schematic* showing the method used to define the distribution of the percentage of Ca^{2+} puffs at the regions exposed to higher LPA concentration (*a*) and the regions exposed to lower LPA concentration (*b*) in relation to the site of the micropipette. *D*, the quantitative analysis of the percentage of Ca^{2+} puffs localized in regions a and b. Data are presented as mean ± S.E. (*error bars*). *E*, LPA gradient-induced differential intracellular Ca^{2+} mobilization in DKO-LPA$_2$ MEFs, not in DKO MEFs. *F*, plot showing the probability of triggering a Ca^{2+} wave by LPA-induced Ca^{2+} puffs in DKO-LPA$_2$ MEFs ($n = 42$). *G*, low frequency Ca^{2+} puffs (<3 Hz) failed to trigger a Ca^{2+} wave. *Scale bar*, 10 μm. *H*, high frequency Ca^{2+} puffs (>5 Hz) triggered a Ca^{2+} wave. *Scale bar*, 10 μm. In *G* and *H*, the circles show the locations of the active Ca^{2+} puff sites. The Ca^{2+} signals recorded at *marked regions* are depicted by the *corresponding traces*. The amplitude is expressed as F/F_0. *F* is the fluorescence intensity in the marked regions where the spark appeared. F_0 is fluorescence intensity of the same area in the absence of Ca^{2+} puffs. The *red arrows* indicate the site with the highest LPA concentration. *IB*, immunoblot.

that mirrored the extracellular LPA gradient. In contrast to DKO-LPA$_2$ MEFs, LPA treatment induced only slight Ca^{2+} mobilization in DKO MEFs (Fig. 3*E*), suggesting that the LPA-induced Ca^{2+} response in DKO-LPA$_2$ MEFs was primarily mediated by activation of LPA$_2$. During the 1-h exposure to an LPA gradient, the global $[Ca^{2+}]_i$ increased and then decreased to create a series of Ca^{2+} oscillations in DKO-LPA$_2$ MEFs (Fig. 3*F*). In each Ca^{2+} oscillation, Ca^{2+} puffs were silenced during and shortly after a Ca^{2+} wave and then arose independently with increasing frequency to trigger the subsequent Ca^{2+} waves. We found that low frequency Ca^{2+} puffs (<3 Hz) often liberated insufficient Ca^{2+} to act as effective triggers of the

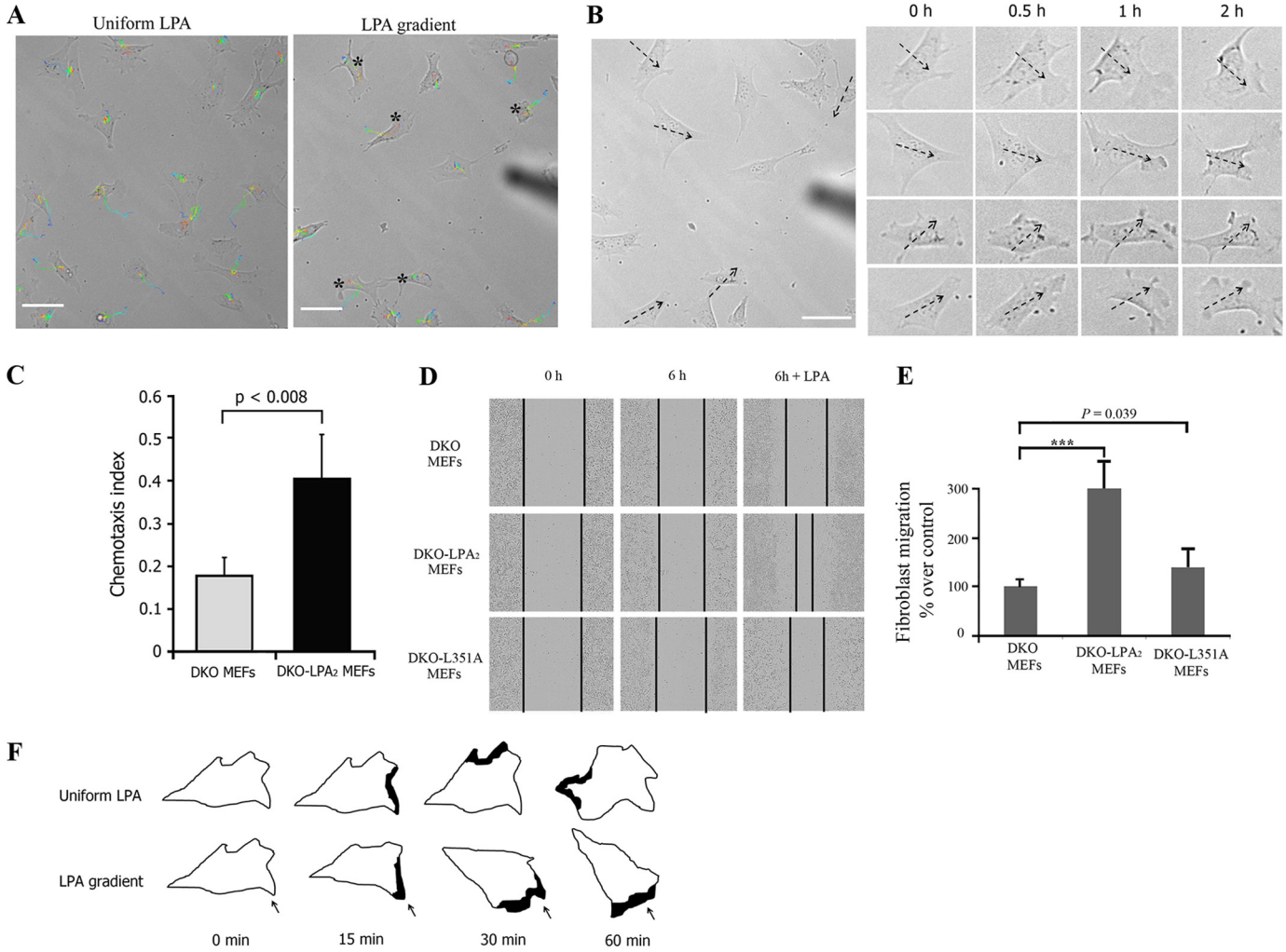

FIGURE 4. **Gradient sensing of fibroblasts stimulated by an LPA gradient.** *A*, representative moving trajectories of DKO-LPA$_2$ MEFs in exposure to an LPA gradient or uniform LPA. The cells were tracked for 1.5 h at a temporal resolution of 1 min/frame. The *black stars* mark cells significantly migrated toward the LPA gradient. The trajectories are *color-coded*. Time information is given by the *color* of the trajectory changing from *blue* (start) to *red* (end). The corresponding videos are available as supplemental Videos 4 and 5. *Scale bar*, 50 μm. *B*, time lapse images of DKO-LPA$_2$ MEFs stimulated with an LPA gradient. The *dashed arrows* point to the direction of higher LPA concentration in the gradient. *Scale bar*, 50 μm. *C*, chemotaxis index of DKO-LPA$_2$ MEFs or DKO MEFs exposed to an LPA gradient. *D*, time lapse images of the wound healing assay in DKO, DKO-LPA$_2$, and DKO-L351A MEF monolayers in the presence or absence of 1 μM LPA. *E*, quantitative analysis of fibroblast migration in a wound healing assay at 6 h postwound in the presence of 1 μM LPA. The data are expressed as the ratios of migratory distance of cells to that of DKO MEFs (mean ± S.E. (*error bars*), $n = 4$). *F*, *schematic representations* showing the formation of protrusions induced by an LPA gradient. In a gradient of LPA, fibroblasts extend new protrusions toward the LPA gradient. When exposed to uniform LPA, fibroblasts extend new protrusions around the entire perimeter of the cell. The *black spot* marks the formation of protrusions. The *arrow* indicates LPA gradient direction.

waves (Fig. 3*G*), and only the high frequency Ca^{2+} puffs (>5 Hz) triggered rapid regenerative Ca^{2+} responses (Fig. 3*H*). Spatially, we observed that Ca^{2+} puffs between a wave and the successive Ca^{2+} wave repeatedly originated in the region proximal to the LPA source. Our results are consistent with a previous finding that the subcellular distribution of Ca^{2+} puff sites determines the spatial patterning of Ca^{2+} signals (35). Thus, recurring spatiotemporal activation of intracellular Ca^{2+} puffs during an oscillation maintained the spatiotemporal Ca^{2+} puff gradient during continuous exposure to an LPA gradient.

LPA$_2$ Mediates Gradient Sensing in Fibroblasts—We used SPT to follow individual cells and calculate the velocity and directionality of migrating DKO-LPA$_2$ MEFs during exposure to an LPA gradient (Fig. 4*A* and supplemental Video 4). A new cell membrane protrusion is the first morphological manifestation of chemotaxis (36). We observed that DKO-LPA$_2$ MEFs extended new protrusions always toward the source of LPA gradient, regardless of whether or not there was a pre-existing protrusion (Fig. 4*B*). In contrast, when LPA was uniformly present in the culture medium, the cells extended protrusions with equal frequency around the entire perimeter of the cells (supplemental Video 5). As shown in Fig. 4*C*, DKO-LPA$_2$ MEFs displayed a high CI, whereas DKO MEFs showed a low CI. In addition, wound healing assays indicated that reconstitution with WT-LPA$_2$ converted DKO MEFs into a highly motile phenotype, confirming that LPA$_2$ enhances LPA-induced fibroblast migration (Fig. 4, *D* and *E*). The spatial correlation of an LPA gradient, cell membrane protrusions, and motility results confirmed that LPA$_2$ is responsible for gradient sensing and directional movement of fibroblasts toward LPA (Fig. 4*F*).

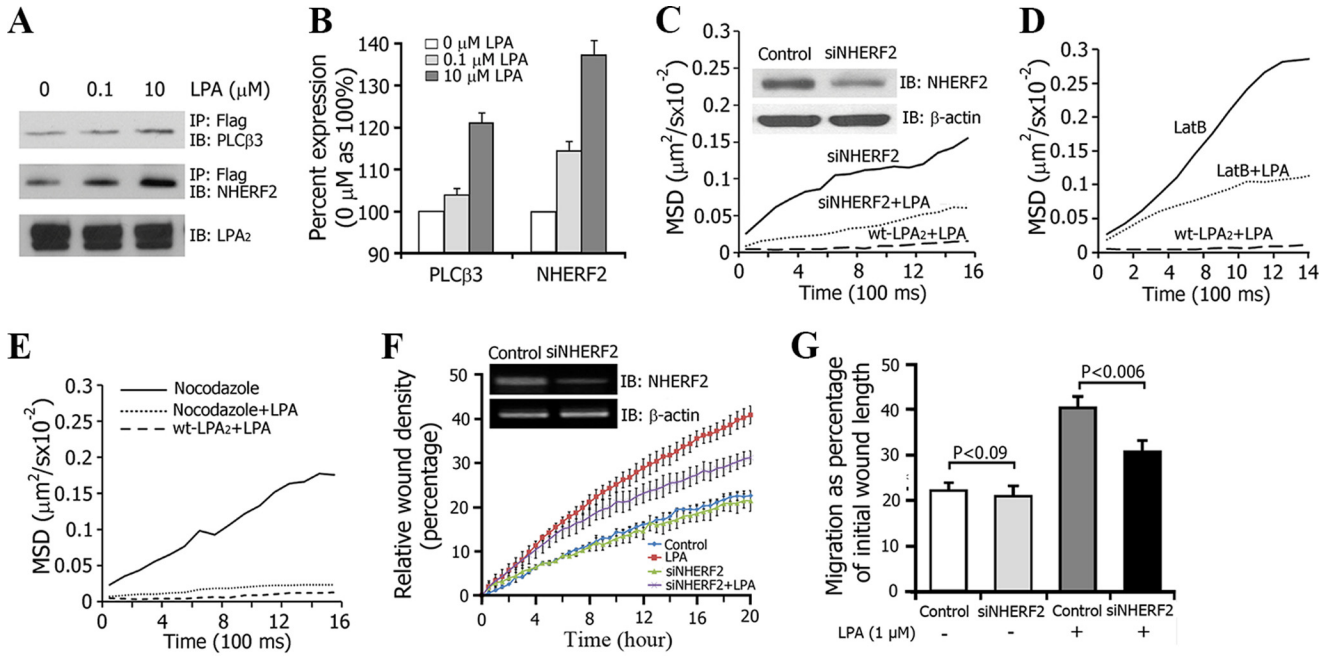

FIGURE 5. **LPA-induced macromolecular complex formation of LPA$_2$ on the plasma membrane.** *A*, co-immunoprecipitation was performed to test the macromolecular complex formation of LPA$_2$, NHERF2, and PLC-β3. *B*, the *bar graph* depicts the average ratios of PLC-β3 and NHERF2 with LPA treatment to their corresponding controls (without LPA treatment). The data are densitometry readings from the immunoreactive bands as represented in *A* (mean ± S.E. (*error bars*), $n = 3$). *C*, MSD *versus* time plots for LPA$_2$ in 3T3-LPA$_2$ cells with or without knockdown of NHERF2 expression and in the presence or absence of LPA. The *inset* blots show the knocking down of NHERF2 expression in 3T3-LPA$_2$ cells. *D*, MSD *versus* time plots of LPA$_2$ in 3T3-LPA$_2$ cells treated with 1 μM LatB for 30 min in the absence or presence of 1 μM LPA. *E*, MSD *versus* time plots of LPA$_2$ in 3T3-LPA$_2$ cells treated with 30 μM nocodazole for 30 min in the absence or presence of 1 μM LPA. *F*, the kinetics of the relative wound density from wound healing assays conducted in the IncuCyte™ high content imaging system. The assays were performed using DKO-LPA$_2$ MEFs with or without transient knockdown of NHERF2 expression. The *inset* blots show the knocking down of NHERF2 expression in DKO-LPA$_2$ MEFs. *G*, quantitative analysis of cells migration as shown in *F*. *IB*, immunoblot.

LPA Induces Assembly of a Macromolecular Complex of LPA$_2$—Ligand binding can reduce the mobility of cell surface receptors by successive coupling to a set of protein partners (37–39). The scaffolding protein NHERF2 specifically binds to the postsynaptic density-95/discs large/zona occludens-1 (PDZ) motif of LPA$_2$ and recruits signaling molecules, including PLC-β3, into a macromolecular complex (40). We observed that LPA exposure increased LPA$_2$·NHERF2·PLC-β3 interactions in a dose-dependent manner (Fig. 5, *A* and *B*). We used siRNA to knock down the endogenous NHERF2 in 3T3-LPA$_2$ cells and monitored the lateral mobility of LPA$_2$. The NHERF2 protein level was reduced by ~70% with siRNA (Fig. 5*C*, *inset*), which significantly increased the lateral mobility of activated LPA$_2$.

Anchoring to the cytoskeleton is one of the major factors that restricts the dynamic mobility of membrane proteins (41). NHERF2 contains a C-terminal ezrin-radixin-moesin (ERM) domain that can link it to the cytoskeleton (42). Disruption of the cytoskeleton using latrunculin B (which inhibits actin polymerization and disrupts microfilament-mediated processes), but not nocodazole (which disrupts microtubules), caused a significant increase in lateral mobility of LPA$_2$ in response to directionally applied LPA (Fig. 5, *D* and *E*). Previous reports have shown that knockdown of NHERF2 decreased cell migration (26, 43). Theisen *et al.* (43) demonstrated that NHERF2·M-cadherin·β-catenin·PDGF receptor macromolecular complexes play an important role in cell motility. Using high content microscopic techniques, we investigated the effect of NHERF2 on the migration of LPA-stimulated DKO-LPA$_2$ MEFs. Transient transfection of these cells with siRNA targeting NHERF2 resulted in an ~70% decrease in the amount of NHERF2 (Fig. 5*F*, *inset*). Wounds were made in confluent monolayers of DKO-LPA$_2$ MEFs, and images were taken at 30-min intervals for up to 24 h. The kinetics of the RWD indicated that knockdown of NHERF2 resulted in slow RWD kinetics with significant reduction of the LPA-stimulated migrations from 40.79 ± 1.79 to 31.18 ± 1.98% ($p < 0.006$) (Fig. 5, *F* and *G*), indicating that knockdown of NHERF2 decreased LPA-induced MEF migration. These observations suggest that the LPA gradient-induced and polarized reduction in the mobility of LPA$_2$ was due to the spatiotemporal assembly of the macromolecular complex linking LPA$_2$ to its binding partners and the cytoskeleton.

LPA$_2$-dependent Cell Migration Requires PLCβ-mediated Activation of Ca^{2+} Microdomains—The role of PLC activation in LPA-mediated migration of intestinal epithelial cells has been demonstrated (44). We examined the functional involvement of PLCβ in LPA-induced fibroblast migration using the PLCβ inhibitor U73122. Treatment of DKO-LPA$_2$ MEFs with U73122 significantly reduced the frequency of LPA-induced Ca^{2+} puffs (Fig. 6*A*). Using high content microscopic techniques, we investigated the regulation of fibroblast migration by PLCβ. The kinetics of the RWD is depicted in Fig. 6*B*. Treatment with U73122 resulted in slow RWD kinetics with significant reduction of the basal migration of DKO-LPA$_2$ MEFs, from 29 ± 1.3 to 17.2 ± 1.1% ($p = 0.002$), and LPA-stimulated migration also was significantly inhibited by U73122, from 40.2 ± 1.8 to 20.6 ± 1.3% ($p < 0.001$) (Fig. 6*C*). These data

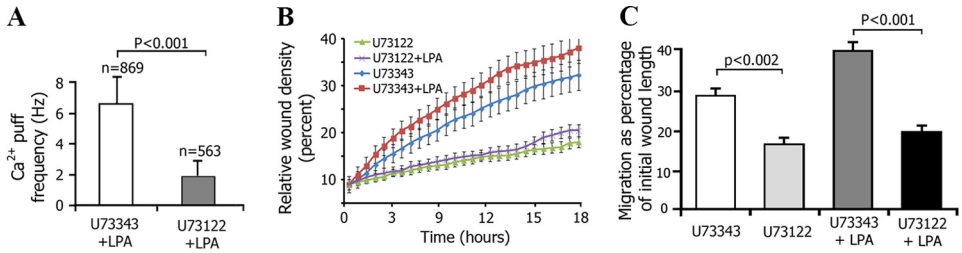

FIGURE 6. **LPA$_2$-dependent cell migration was inhibited by a PLC-β inhibitor.** *A*, frequency of LPA-induced Ca^{2+} puffs in DKO-LPA$_2$ MEFs treated with PLC-β inhibitor U73122 (2 μM) or its inactive analog U73343 (2 μM). *B*, kinetics of the relative wound density in the presence of U73122 (2 μM), U73343 (2 μM), or either U73122 or U73343 plus LPA (1 μM). The data were analyzed using IncuCyte^{TM} software. *C*, the migration of DKO-LPA$_2$ MEFs at the basal or LPA-activated state with U73122 (2 μM) or U73343 (2 μM) treatment. *Error bars*, S.E.

suggest that generation of LPA$_2$-mediated Ca^{2+} puffs and fibroblast migration require PLCβ activity.

Disruption of the PDZ Motif Attenuates the LPA Gradient-induced Spatiotemporal Organization of Ca^{2+} Puffs and Impairs Gradient Sensing of Fibroblasts—The intracellular C-terminal PDZ motif of LPA$_2$ plays an important role in the regulation of LPA$_2$-mediated signaling (45). We reconstituted 3T3 cells with the L351A-LPA$_2$ mutant, which has a leucine-to-alanine mutation in the PDZ motif that renders it inactive to forming PDZ motif-dependent complexes. We found that this mutation increased the D_{med} of activated LPA$_2$ ~5.5-fold, from 0.0023 ± 0.0012 to 0.0128 ± 0.0025 $\mu m^2/s$. However, this mutant had no effect on the D_{med} of the receptor in its basal state (Fig. 7, *A* and *B*). In the presence of an LPA gradient, the mobility of the L351A mutant was indistinguishable between the proximal portion and the distal portion relative to the LPA source (Fig. 7*C*), which suggested that the PDZ motif of LPA$_2$ is required for the spatial macromolecular complex formation of LPA$_2$ and tightly regulates the lateral mobility of activated LPA$_2$.

We also reconstituted DKO MEFs with the L351A-LPA$_2$ (DKO-L351A MEFs). Disruption of the PDZ motif caused a 21.3% reduction in the frequency (Fig. 7*D*) and a 38.2% reduction in the amplitude (Fig. 7*E*) of Ca^{2+} puffs. After exposure to an LPA gradient, The occurrence difference of Ca^{2+} puffs in regions a and b of DKO-L351A cells is not significant (Fig. 7*F*), contrary to that in DKO LPA$_2$ MEF (Fig. 3*D*). Also, fewer Ca^{2+} puffs were initiated in region a of DKO-L351A MEFs compared with that of DKO-LPA$_2$ MEFs. Thus, disruption of the PDZ motif attenuated the sensitivity of fibroblasts to an LPA gradient. In addition, DKO-L351A MEFs exhibited a low CI compared with DKO-LPA$_2$ MEFs (Fig. 7*G*). Taken together, our data suggest that the PDZ motif-mediated asymmetric macromolecular complex assembly of LPA$_2$ regulates the gradient sensing of fibroblasts.

DISCUSSION

Based on our findings, we propose that LPA gradient sensing in fibroblasts is mediated by spatially organized, PDZ motif-mediated assembly of macromolecular complexes of LPA$_2$ on the plasma membrane, which causes asymmetric intracellular Ca^{2+} signals to govern directional migration of fibroblasts (Fig. 8).

Chemoattractant receptors are uniformly distributed along the plasma membrane during random or chemotactic movement, even when cells are induced to reverse direction or turn by repositioning the micropipette filled with the chemoattractant cue (7). The even distribution of the chemoattractant receptors is consistent with the fact that fibroblasts are chemotactically responsive at all points on their perimeter and, thereby, suited for gradient sensing through a spatial mechanism. To answer the question of at what point in the signaling pathway a response becomes localized, we used SPT techniques to visualize that an LPA gradient caused a spatially restricted activation of LPA$_2$ along the plasma membrane although this receptor was uniformly distributed. Our data demonstrate that LPA affected the lateral diffusion of LPA$_2$ within milliseconds. Although fibroblasts move far more slowly than of cells of *Dictyostelium* and neutrophils, we found that gradient sensing of fibroblasts is rapidly processed. Swanson *et al.* (46) observed that chemotaxing cells respond with an L-shaped turn of the pseudopod, instead of reorganizing the morphological polarization, when a cAMP-loaded microneedle producing the gradient is shifted to the side of the cell. FRET studies between the G-protein subunits revealed a higher GPCR-mediated activation at the leading edge of *Dictyostelium* cells within milliseconds (47). de Keijzer *et al.* (13) have reported that a spatially restricted increase in receptor mobility is involved in directional sensing during *D. discoideum* chemotaxis, and they observed high spatial and temporal mobility of cAMP receptor 1 within milliseconds. These observations suggest that gradient sensing occurs rapidly (within milliseconds), which strengthens our contention that the rapid changes in LPA$_2$-mediated receptor mobility we observed provide evidence as to the mechanism of how gradient sensing occurs in fibroblasts.

Gradient sensing depends on the translation of an external gradient into an amplified intracellular signal gradient (48). This signaling asymmetry leads to an asymmetry in cell shape accomplished by cytoskeleton rearrangement. Care is needed to distinguish the differences among gradient sensing, morphological polarization, and directional migration. Morphological polarity is a passive readout for chemotaxis in eukaryotic cells (6, 49–51) but not a requirement for gradient sensing (50). Similarly, the inability to move in a given direction tells nothing about the capability to sense that direction. Experiments using latrunculin A have shown that morphologically unpolarized, immobile *Dictyostelium* cells can still sense a cAMP gradient (49, 52). Cells tend to maintain their once established polarity even when the direction of the gradient is altered.

Our results support the hypothesis that spatiotemporal (asymmetric) macromolecular complex formation of LPA$_2$ ini-

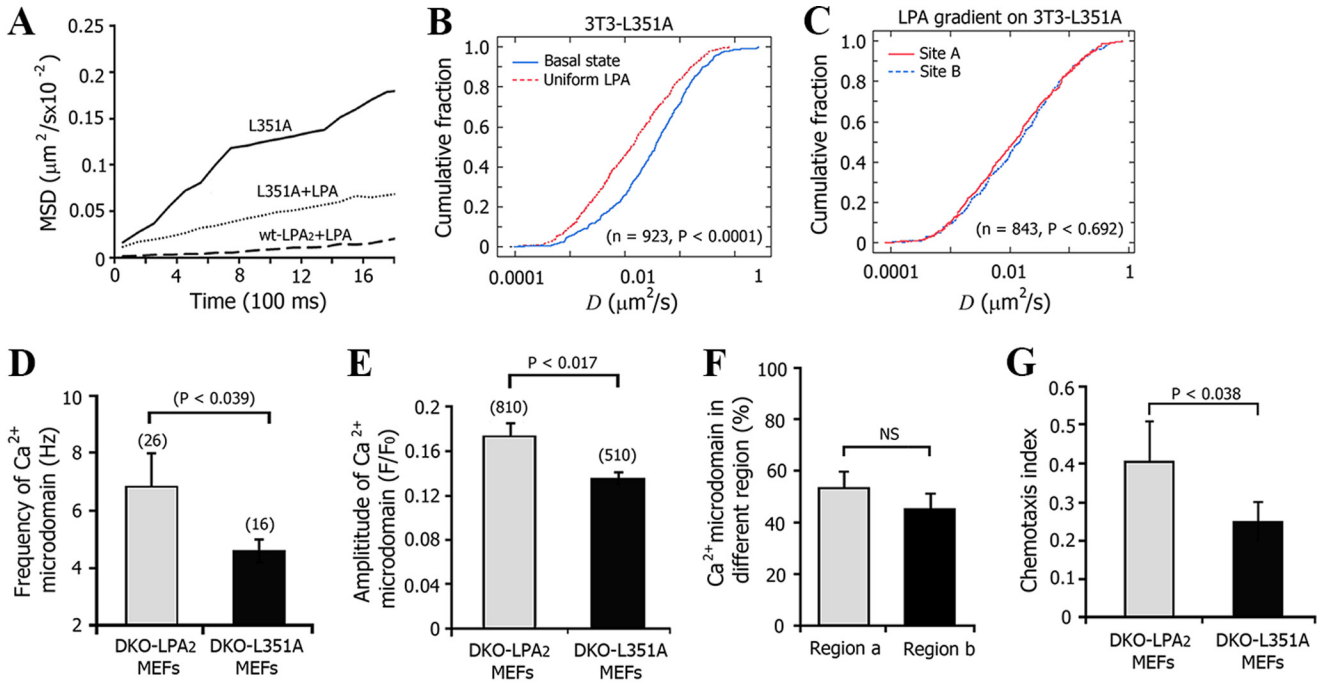

FIGURE 7. **Disruption of the PDZ motif of LPA$_2$ attenuated the LPA gradient-induced spatial decrease in LPA$_2$ mobility.** *A*, MSD *versus* time plots for LPA$_2$-L351A and WT-LPA$_2$ expressed in 3T3 cells treated with or without 1 μM LPA. *B*, comparison of cumulative fraction plots from the KS-test of the difference in the diffusion coefficient of lateral L351A at basal and uniform LPA-activated state. The respective number of trajectories (*n*) and *p* value are listed. *C*, KS-test of the difference in the diffusion coefficient of lateral L351A mutant at sites A and B after exposure to an LPA gradient. *D*, frequency of Ca^{2+} puffs in DKO LPA$_2$ or DKO-L351A MEFs. The number of cells tested is indicated *above* each *bar*. Data are presented as mean ± S.E. (*error bars*). *E*, mean amplitude of Ca^{2+} puffs in DKO-LPA$_2$ or DKO-L351A MEFs. The number of Ca^{2+} puffs tested is indicated *above* each *bar*. *F*, quantitative analysis of the percentage of Ca^{2+} puffs localized in region a (close to the micropipette) and region b (away from the micropipette) in DKO-L351A MEFs. Data are presented as mean ± S.E., $n = 42$. *G*, chemotaxis index from DKO-L351A MEFs compared with DKO-LPA2 MEFs upon exposure to an LPA gradient.

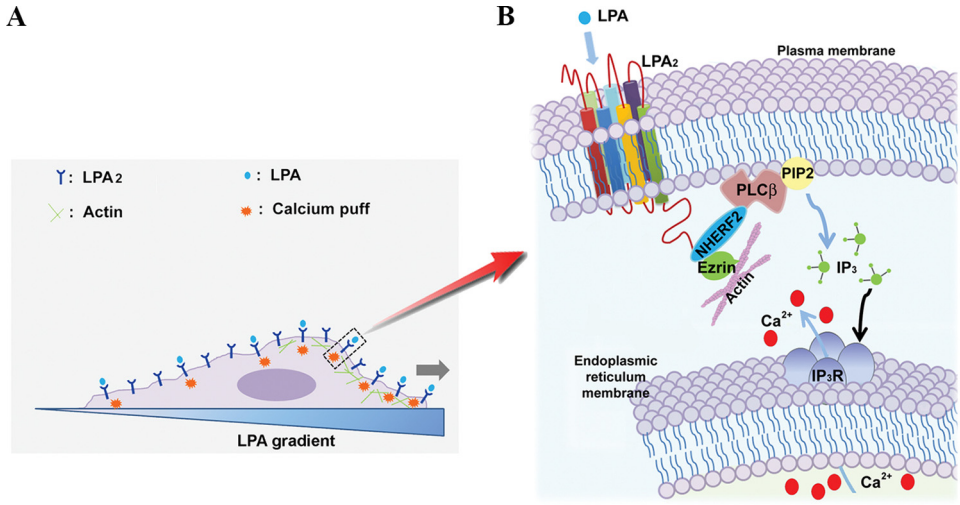

FIGURE 8. **A proposed model to depict the mechanism underlying the LPA$_2$-mediated gradient sensing and migration of fibroblasts in response to an extracellular LPA cue.** *A*, a schematic representation of asymmetric Ca^{2+} puff activation in cells exposed to an LPA gradient. *B*, LPA-induced and LPA$_2$-mediated gradient sensing of fibroblasts is initiated through the asymmetric formation of LPA$_2$ complexes, which activate downstream asymmetric PLC-β3-inositol 1,4,5-trisphosphate/Ca^{2+} signaling to trigger Ca^{2+} puffs to guide the gradient sensing and migration of fibroblasts.

tiates the translation of an external LPA gradient. The next question to be answered is what downstream process carries the signal amplification and eventually directs gradient sensing of fibroblasts. LPA induces mobilization of intracellular Ca^{2+} (53), and Ca^{2+} plays a multifunctional role in gradient sensing, cytoskeleton redistribution, and relocation of focal adhesion (19, 54, 55). The signaling and motility center, the leading lamella, contains numerous effector proteins that require high levels of calcium for activation (56, 57). However, intracellular Ca^{2+} displays a rear-to-front gradient, and transient increases of Ca^{2+} concentration have been observed in migrating cells; they are infrequent and mainly localized in the tail of the cell (20). Recently, Wei *et al.* (21) showed that spatially and temporally restricted flickers of Ca^{2+} signaling are enriched near the leading edge of motile fibroblasts. Also, the difference in the integrated intensity of Ca^{2+} flickers on one side of the leading

edge *versus* the other correlates strongly with the turning behavior of the cells (58). We visualized that an LPA gradient induced a spatial-temporal distribution of Ca^{2+} puff sites, which determined the spatial patterning of Ca^{2+} signals and then steered cell migration. These observations suggest that localized Ca^{2+} elevation may be responsible for the local Ca^{2+}-dependent events at the front of cells. In addition, we also observed that the slight initial asymmetric Ca^{2+} puff activity resulted in significantly higher Ca^{2+} puffs and then global Ca^{2+} mobilization within minutes, which may be the positive feedback loop for LPA-induced migration. Moreover, it will be important to investigate the immediate signaling events activated locally by a Ca^{2+} puff, such as local polymerization and depolymerization of cytoskeletal filaments or activation of Ca^{2+} signaling proteins in these Ca^{2+} microdomains. Although there have been several prior studies focusing on intracellular signaling pathways that positively or negatively regulate cell migration, few studies have addressed mechanisms regulating the gradient sensing and chemotactic response to LPA in fibroblasts. Our observations unveil a molecular mechanism to explain which factors act upstream to transmit extracellular chemoattractant signals into intracellular signals and which factors act downstream to transduce these signals into mechanical forces.

The next question to be answered is how LPA-induced rapid changes in LPA_2 mobility and rapid Ca^{2+} dynamics (*i.e.* within milliseconds) in defined regions of the cells lead to the observed rather slower migration of fibroblasts (*i.e.* within hours). When we maintained the LPA gradient, the asymmetric pattern of receptor mobility was observed. During the 1-h exposure to an LPA gradient, the global $[Ca^{2+}]_i$ increased and then decreased to create a series of Ca^{2+} oscillations. In each Ca^{2+} oscillation, Ca^{2+} puffs were silenced during and shortly after a Ca^{2+} wave and then arose independently with increasing frequency to trigger the subsequent Ca^{2+} waves, and thereby, the spatiotemporal patterns of Ca^{2+} puffs were maintained. Thus, recurring spatiotemporal activation of intracellular Ca^{2+} puffs during an oscillation can maintain the spatiotemporal Ca^{2+} puff gradient during continuous exposure to an LPA gradient. These local events would interact with self-organizing systems that drive motility through global polarization and locally propagating waves of actin nucleation to bias cell migration toward the source of the chemoattractant.

The observed spatially restricted mobility of LPA_2 was a result of PDZ motif-mediated coupling with downstream signaling partners to form an LPA_2·NHERF2·PLC-β3 macromolecular complex that anchors to the cytoskeleton (59). LPA gradient-induced spatial (asymmetric) activation of LPA_2 could account for the primary event, which then elicits the downstream asymmetric signaling pathway needed for gradient sensing of fibroblasts. The SPT data provide the first evidence that the mobility of the chemoattractant receptor is directly involved in gradient sensing in fibroblasts. Thus, spatially localized activation of LPA_2 restricts its membrane mobility via the PDZ-mediated recruitment of NHERF2·PLC-β3-coupled Ca^{2+} microdomains and cytoskeletal interaction that in turn govern directional migration of fibroblasts.

We observed that a macromolecular complex, including PLC-β3 assembled with LPA_2, is required for triggering asymmetric distribution of Ca^{2+} puffs. Disruption of this PDZ motif-mediated complex of LPA_2 attenuated the intracellular Ca^{2+} puff gradient, impaired fibroblast gradient sensing, and consequently reduced directional fibroblast migration. Our data demonstrate that treatment of DKO-LPA_2 MEFs with PLCβ inhibitor U73122 significantly inhibited LPA-induced Ca^{2+} puff frequency as well as basal and LPA-stimulated cell migration. Frequency of Ca^{2+} puffs >5 Hz and spatially organized by the macromolecular complex triggered Ca^{2+} waves leading to directional activation of Ca^{2+}-dependent downstream migratory signaling in the cell. Our data indicate the frequency of Ca^{2+} microdomain signaling as the dynamic process of signal amplification when a cell encounters an LPA gradient. Ca^{2+} influx during growth cone attraction is mediated by transient receptor potential channels, a class of Ca^{2+}-permeable receptor-operated channels (60, 61). A recent study showed that NHERF2 and TRPC4 (transient receptor potential channel 4) influence Ca^{2+} signaling (62), making it possible that Ca^{2+} influx contributes in part to the amplification of local Ca^{2+} levels. Further experiments will be needed to confirm this hypothesis.

Gradient sensing is a crucial step during cell chemotaxis, and LPA has been shown to contribute to fibroblast recruitment induced by lung injury (63). Recent studies also have established that LPA_2 mediates the migration of several types of cancer cells (26–28). Because most mammalian cell types are LPA-responsive, our findings may unveil a more general role for LPA_2 in different pathological events, including cancer invasion and metastasis.

Acknowledgments—We thank Dr. David L. Armbruster for critical reading of the manuscript. We are grateful to J. Denise Wetzel (Cincinnati Children's Hospital Medical Center) for critical review of the manuscript.

REFERENCES

1. Cha, I., Lee, S. H., and Jeon, T. J. (2010) Chemoattractant-mediated Rap1 activation requires GPCR/G proteins. *Mol. Cells* **30,** 563–567
2. Postma, M., Bosgraaf, L., Loovers, H. M., and Van Haastert, P. J. (2004) Chemotaxis: signalling modules join hands at front and tail. *EMBO Rep.* **5,** 35–40
3. Iijima, M., Huang, Y. E., and Devreotes, P. (2002) Temporal and spatial regulation of chemotaxis. *Dev. Cell* **3,** 469–478
4. Jasuja, R., Lin, Y., Trentham, D. R., and Khan, S. (1999) Response tuning in bacterial chemotaxis. *Proc. Natl. Acad. Sci. U.S.A.* **96,** 11346–11351
5. Devreotes, P., and Janetopoulos, C. (2003) Eukaryotic chemotaxis: distinctions between directional sensing and polarization. *J. Biol. Chem.* **278,** 20445–20448
6. Jin, T., Zhang, N., Long, Y., Parent, C. A., and Devreotes, P. N. (2000) Localization of the G protein betagamma complex in living cells during chemotaxis. *Science* **287,** 1034–1036
7. Xiao, Z., Zhang, N., Murphy, D. B., and Devreotes, P. N. (1997) Dynamic distribution of chemoattractant receptors in living cells during chemotaxis and persistent stimulation. *J. Cell Biol.* **139,** 365–374
8. Schwarz-Romond, T., and Gorski, S. A. (2010) Focus on the spatial organization of signalling. *EMBO J.* **29,** 2675–2676
9. Parent, C. A., and Devreotes, P. N. (1999) A cell's sense of direction. *Science* **284,** 765–770
10. Xu, X., Meier-Schellersheim, M., Jiao, X., Nelson, L. E., and Jin, T. (2005)

Quantitative imaging of single live cells reveals spatiotemporal dynamics of multistep signaling events of chemoattractant gradient sensing in *Dictyostelium*. *Mol. Biol. Cell* **16,** 676–688
11. Xu, X., Meckel, T., Brzostowski, J. A., Yan, J., Meier-Schellersheim, M., and Jin, T. (2010) Coupling mechanism of a GPCR and a heterotrimeric G protein during chemoattractant gradient sensing in *Dictyostelium*. *Sci. Signal.* **3,** ra71
12. Ueda, M., Sako, Y., Tanaka, T., Devreotes, P., and Yanagida, T. (2001) Single-molecule analysis of chemotactic signaling in *Dictyostelium* cells. *Science* **294,** 864–867
13. de Keijzer, S., Sergé, A., van Hemert, F., Lommerse, P. H., Lamers, G. E., Spaink, H. P., Schmidt, T., and Snaar-Jagalska, B. E. (2008) A spatially restricted increase in receptor mobility is involved in directional sensing during *Dictyostelium discoideum* chemotaxis. *J. Cell Sci.* **121,** 1750–1757
14. Funamoto, S., Meili, R., Lee, S., Parry, L., and Firtel, R. A. (2002) Spatial and temporal regulation of 3-phosphoinositides by PI 3-kinase and PTEN mediates chemotaxis. *Cell* **109,** 611–623
15. Ferguson, G. J., Milne, L., Kulkarni, S., Sasaki, T., Walker, S., Andrews, S., Crabbe, T., Finan, P., Jones, G., Jackson, S., Camps, M., Rommel, C., Wymann, M., Hirsch, E., Hawkins, P., and Stephens, L. (2007) PI(3)Kγ has an important context-dependent role in neutrophil chemokinesis. *Nat. Cell Biol.* **9,** 86–91
16. Loovers, H. M., Postma, M., Keizer-Gunnink, I., Huang, Y. E., Devreotes, P. N., and van Haastert, P. J. (2006) Distinct roles of PI(3,4,5)P3 during chemoattractant signaling in *Dictyostelium*: a quantitative *in vivo* analysis by inhibition of PI3-kinase. *Mol. Biol. Cell* **17,** 1503–1513
17. Wu, H., Goel, V., and Haluska, F. G. (2003) PTEN signaling pathways in melanoma. *Oncogene* **22,** 3113–3122
18. Chen, L., Iijima, M., Tang, M., Landree, M. A., Huang, Y. E., Xiong, Y., Iglesias, P. A., and Devreotes, P. N. (2007) PLA2 and PI3K/PTEN pathways act in parallel to mediate chemotaxis. *Dev. Cell* **12,** 603–614
19. Ridley, A. J., Schwartz, M. A., Burridge, K., Firtel, R. A., Ginsberg, M. H., Borisy, G., Parsons, J. T., and Horwitz, A. R. (2003) Cell migration: integrating signals from front to back. *Science* **302,** 1704–1709
20. Brundage, R. A., Fogarty, K. E., Tuft, R. A., and Fay, F. S. (1991) Calcium gradients underlying polarization and chemotaxis of eosinophils. *Science* **254,** 703–706
21. Wei, C., Wang, X., Chen, M., Ouyang, K., Song, L. S., and Cheng, H. (2009) Calcium flickers steer cell migration. *Nature* **457,** 901–905
22. Henley, J. R., Huang, K. H., Wang, D., and Poo, M. M. (2004) Calcium mediates bidirectional growth cone turning induced by myelin-associated glycoprotein. *Neuron* **44,** 909–916
23. Blaser, H., Reichman-Fried, M., Castanon, I., Dumstrei, K., Marlow, F. L., Kawakami, K., Solnica-Krezel, L., Heisenberg, C. P., and Raz, E. (2006) Migration of zebrafish primordial germ cells: a role for myosin contraction and cytoplasmic flow. *Dev. Cell* **11,** 613–627
24. Evans, J. H., and Falke, J. J. (2007) Ca^{2+} influx is an essential component of the positive-feedback loop that maintains leading-edge structure and activity in macrophages. *Proc. Natl. Acad. Sci. U.S.A.* **104,** 16176–16181
25. Choi, J. W., Herr, D. R., Noguchi, K., Yung, Y. C., Lee, C. W., Mutoh, T., Lin, M. E., Teo, S. T., Park, K. E., Mosley, A. N., and Chun, J. (2010) LPA receptors: subtypes and biological actions. *Annu. Rev. Pharmacol. Toxicol.* **50,** 157–186
26. Lee, S. J., Ritter, S. L., Zhang, H., Shim, H., Hall, R. A., and Yun, C. C. (2011) MAGI-3 competes with NHERF-2 to negatively regulate LPA2 receptor signaling in colon cancer cells. *Gastroenterology* **140,** 924–934
27. Chen, M., Towers, L. N., and O'Connor, K. L. (2007) LPA2 (EDG4) mediates Rho-dependent chemotaxis with lower efficacy than LPA1 (EDG2) in breast carcinoma cells. *Am. J. Physiol. Cell Physiol.* **292,** C1927–C1933
28. Hasegawa, Y., Murph, M., Yu, S., Tigyi, G., and Mills, G. B. (2008) Lysophosphatidic acid (LPA)-induced vasodilator-stimulated phosphoprotein mediates lamellipodia formation to initiate motility in PC-3 prostate cancer cells. *Mol. Oncol.* **2,** 54–69
29. E, S., Lai, Y. J., Tsukahara, R., Chen, C. S., Fujiwara, Y., Yue, J., Yu, J. H., Guo, H., Kihara, A., Tigyi, G., and Lin, F. T. (2009) Lysophosphatidic acid 2 receptor-mediated supramolecular complex formation regulates its antiapoptotic effect. *J. Biol. Chem.* **284,** 14558–14571
30. Sinha, C., Ren, A., Arora, K., Moon, C. S., Yarlagadda, S., Zhang, W., Cheepala, S. B., Schuetz, J. D., and Naren, A. P. (2013) Multi-drug resistance protein 4 (MRP4)-mediated regulation of fibroblast cell migration reflects a dichotomous role of intracellular cyclic nucleotides. *J. Biol. Chem.* **288,** 3786–3794
31. Wessels, D., Lusche, D. F., Kuhl, S., Heid, P., and Soll, D. R. (2007) PTEN plays a role in the suppression of lateral pseudopod formation during Dictyostelium motility and chemotaxis. *J. Cell Sci.* **120,** 2517–2531
32. Wang, D. A., Lorincz, Z., Bautista, D. L., Liliom, K., Tigyi, G., and Parrill, A. L. (2001) A single amino acid determines lysophospholipid specificity of the S1P1 (EDG1) and LPA1 (EDG2) phospholipid growth factor receptors. *J. Biol. Chem.* **276,** 49213–49220
33. Meyer Zu Heringdorf, D. (2004) Lysophospholipid receptor-dependent and -independent calcium signaling. *J. Cell. Biochem.* **92,** 937–948
34. Contos, J. J., Ishii, I., Fukushima, N., Kingsbury, M. A., Ye, X., Kawamura, S., Brown, J. H., and Chun, J. (2002) Characterization of lpa(2) (Edg4) and lpa(1)/lpa(2) (Edg2/Edg4) lysophosphatidic acid receptor knockout mice: signaling deficits without obvious phenotypic abnormality attributable to lpa(2). *Mol. Cell. Biol.* **22,** 6921–6929
35. Marchant, J. S., and Parker, I. (2001) Role of elementary Ca^{2+} puffs in generating repetitive Ca^{2+} oscillations. *EMBO J.* **20,** 65–76
36. Mouneimne, G., Soon, L., DesMarais, V., Sidani, M., Song, X., Yip, S. C., Ghosh, M., Eddy, R., Backer, J. M., and Condeelis, J. (2004) Phospholipase C and cofilin are required for carcinoma cell directionality in response to EGF stimulation. *J. Cell Biol.* **166,** 697–708
37. Schaaf, M. J., and Cidlowski, J. A. (2003) Molecular determinants of glucocorticoid receptor mobility in living cells: the importance of ligand affinity. *Mol. Cell. Biol.* **23,** 1922–1934
38. Ali, G. S., Prasad, K. V., Day, I., and Reddy, A. S. (2007) Ligand-dependent reduction in the membrane mobility of FLAGELLIN SENSITIVE2, an *Arabidopsis* receptor-like kinase. *Plant Cell Physiol.* **48,** 1601–1611
39. Plested, A. J., and Mayer, M. L. (2009) AMPA receptor ligand binding domain mobility revealed by functional cross-linking. *J. Neurosci.* **29,** 11912–11923
40. Oh, Y. S., Jo, N. W., Choi, J. W., Kim, H. S., Seo, S. W., Kang, K. O., Hwang, J. I., Heo, K., Kim, S. H., Kim, Y. H., Kim, I. H., Kim, J. H., Banno, Y., Ryu, S. H., and Suh, P. G. (2004) NHERF2 specifically interacts with LPA2 receptor and defines the specificity and efficiency of receptor-mediated phospholipase C-β3 activation. *Mol. Cell. Biol.* **24,** 5069–5079
41. Saxton, M. J., and Jacobson, K. (1997) Single-particle tracking: applications to membrane dynamics. *Annu. Rev. Biophys. Biomol. Struct.* **26,** 373–399
42. Shenolikar, S., and Weinman, E. J. (2001) NHERF: targeting and trafficking membrane proteins. *Am. J. Physiol. Renal Physiol.* **280,** F389–F395
43. Theisen, C. S., Wahl, J. K., 3rd, Johnson, K. R., and Wheelock, M. J. (2007) NHERF links the N-cadherin/catenin complex to the platelet-derived growth factor receptor to modulate the actin cytoskeleton and regulate cell motility. *Mol. Biol. Cell* **18,** 1220–1232
44. Lee, S. J., Leoni, G., Neumann, P. A., Chun, J., Nusrat, A., and Yun, C. C. (2013) Distinct phospholipase C-β isozymes mediate lysophosphatidic acid receptor 1 effects on intestinal epithelial homeostasis and wound closure. *Mol. Cell. Biol.* **33,** 2016–2028
45. Lin, F. T., and Lai, Y. J. (2008) Regulation of the LPA2 receptor signaling through the carboxyl-terminal tail-mediated protein-protein interactions. *Biochim. Biophys. Acta* **1781,** 558–562
46. Swanson, J. A., and Taylor, D. L. (1982) Local and spatially coordinated movements in *Dictyostelium discoideum* amoebae during chemotaxis. *Cell* **28,** 225–232
47. Xu, X., Brzostowski, J. A., and Jin, T. (2009) Monitoring dynamic GPCR signaling events using fluorescence microscopy, FRET imaging, and single-molecule imaging. *Methods Mol. Biol.* **571,** 371–383
48. von Philipsborn, A., and Bastmeyer, M. (2007) Mechanisms of gradient detection: a comparison of axon pathfinding with eukaryotic cell migration. *Int. Rev. Cytol.* **263,** 1–62
49. Servant, G., Weiner, O. D., Herzmark, P., Balla, T., Sedat, J. W., and Bourne, H. R. (2000) Polarization of chemoattractant receptor signaling during neutrophil chemotaxis. *Science* **287,** 1037–1040
50. Rubin, H., and Ravid, S. (2002) Polarization of myosin II heavy chain-protein kinase C in chemotaxing *Dictyostelium* cells. *J. Biol. Chem.* **277,**

36005–36008
51. Parent, C. A., Blacklock, B. J., Froehlich, W. M., Murphy, D. B., and Devreotes, P. N. (1998) G protein signaling events are activated at the leading edge of chemotactic cells. *Cell* **95,** 81–91
52. Janetopoulos, C., Ma, L., Devreotes, P. N., and Iglesias, P. A. (2004) Chemoattractant-induced phosphatidylinositol 3,4,5-trisphosphate accumulation is spatially amplified and adapts, independent of the actin cytoskeleton. *Proc. Natl. Acad. Sci. U.S.A.* **101,** 8951–8956
53. Hildebrandt, J. P. (1995) Lysophosphatidic acid induces inositol phosphate and calcium signals in exocrine cells from the avian nasal salt gland. *J. Membr. Biol.* **144,** 49–58
54. Van Haastert, P. J., and Devreotes, P. N. (2004) Chemotaxis: signalling the way forward. *Nat. Rev. Mol. Cell Biol.* **5,** 626–634
55. Lee, J., Ishihara, A., Oxford, G., Johnson, B., and Jacobson, K. (1999) Regulation of cell movement is mediated by stretch-activated calcium channels. *Nature* **400,** 382–386
56. Stossel, T. P., Fenteany, G., and Hartwig, J. H. (2006) Cell surface actin remodeling. *J. Cell Sci.* **119,** 3261–3264
57. Franco, S. J., Rodgers, M. A., Perrin, B. J., Han, J., Bennin, D. A., Critchley, D. R., and Huttenlocher, A. (2004) Calpain-mediated proteolysis of talin regulates adhesion dynamics. *Nat. Cell Biol.* **6,** 977–983
58. Wei, C., Wang, X., Chen, M., Ouyang, K., Zheng, M., and Cheng, H. (2010) Flickering calcium microdomains signal turning of migrating cells. *Can. J. Physiol. Pharmacol.* **88,** 105–110
59. Cao, T. T., Deacon, H. W., Reczek, D., Bretscher, A., and von Zastrow, M. (1999) A kinase-regulated PDZ-domain interaction controls endocytic sorting of the β2-adrenergic receptor. *Nature* **401,** 286–290
60. Li, Y., Jia, Y. C., Cui, K., Li, N., Zheng, Z. Y., Wang, Y. Z., and Yuan, X. B. (2005) Essential role of TRPC channels in the guidance of nerve growth cones by brain-derived neurotrophic factor. *Nature* **434,** 894–898
61. Shim, S., Goh, E. L., Ge, S., Sailor, K., Yuan, J. P., Roderick, H. L., Bootman, M. D., Worley, P. F., Song, H., and Ming, G. L. (2005) XTRPC1-dependent chemotropic guidance of neuronal growth cones. *Nat. Neurosci.* **8,** 730–735
62. Lee-Kwon, W., Wade, J. B., Zhang, Z., Pallone, T. L., and Weinman, E. J. (2005) Expression of TRPC4 channel protein that interacts with NHERF-2 in rat descending vasa recta. *Am. J. Physiol. Cell Physiol.* **288,** C942–C949
63. Tager, A. M., LaCamera, P., Shea, B. S., Campanella, G. S., Selman, M., Zhao, Z., Polosukhin, V., Wain, J., Karimi-Shah, B. A., Kim, N. D., Hart, W. K., Pardo, A., Blackwell, T. S., Xu, Y., Chun, J., and Luster, A. D. (2008) The lysophosphatidic acid receptor LPA1 links pulmonary fibrosis to lung injury by mediating fibroblast recruitment and vascular leak. *Nat. Med.* **14,** 45–54